City Research Online

City, University of London Institutional Repository

This is the published version of the paper.

This version of the publication may differ from the final published version.

On-chip supercontinuum generation in nanostructured Ge$_{11.5}$As$_{24}$Se$_{64.5}$ chalcogenide waveguides using Panda-ring resonator

S. Suwanarat[a], S. Chiangga[b], I.S. Amiri[c], S.Z. Haider[d], M.S. Aziz[d], J. Ali[d], G. Singh[e], R. Poznanski[f], P. Yupapin[g,h,*], K.T.V. Grattan[i]

[a] *Department of Physics, Faculty of Science, Ramkhamheang University, Bangkok 1220, Thailand*
[b] *Department of Physics, Faculty of Science, Kasetsart University, Bangkok 1090, Thailand*
[c] *Division of Materials Science and Engineering, Boston University, Boston, MA 02215, USA*
[d] *Laser Center, Ibnu Sina ISIR, Universiti Teknologi Malaysia, 81310, Malaysia*
[e] *Department of Electronics and Communication Engineering, Malaviya National Institute of Technology Jaipur, India*
[f] *I-CODE, Universiti Sultan Zainal Abidin, 21300 Kuala Nerus, Terengganu, Malaysia*
[g] *Computational Optics Research Group, Advanced Institute of Materials Science, Ton Duc Thang University, District 7, Ho Chi Minh City, Viet Nam*
[h] *Faculty of Electrical & Electronics Engineering, Ton Duc Thang University, District 7, Ho Chi Minh City, Viet Nam*
[i] *Department of Electrical & Electronic Engineering, School of Mathematics, Computer Science and Engineering, The City, University of London, London, UK*

ABSTRACT

The on-chip scale microring circuit is proposed to numerically investigate the supercontinuum (SC) generation of light power. The device is formed by the chalcogenide Panda-ring resonator with the nanoscale planar waveguide using Ge$_{11.5}$As$_{24}$Se$_{64.5}$ chalcogenide glass channel waveguide, air-clad and MgF$_2$ glass for lower cladding. The waveguide is designed to exhibit normal dispersion along with a low-energy pumped at 1.55 μm using a short pulse, which has the duration of 50 fs and peak power ranging from 1 W to 100 W. The numerical result obtained has shown a good-quality SC generation of both the spectral bandwidth and high output peak power. All SC spectral extended to more than 13 μm by cumulative Kerr nonlinearities. The obtained results can be useful for developing new experimental work in the important area of SC generation on compact chip broadband sources, which can be used in both infrared and radio wave applications.
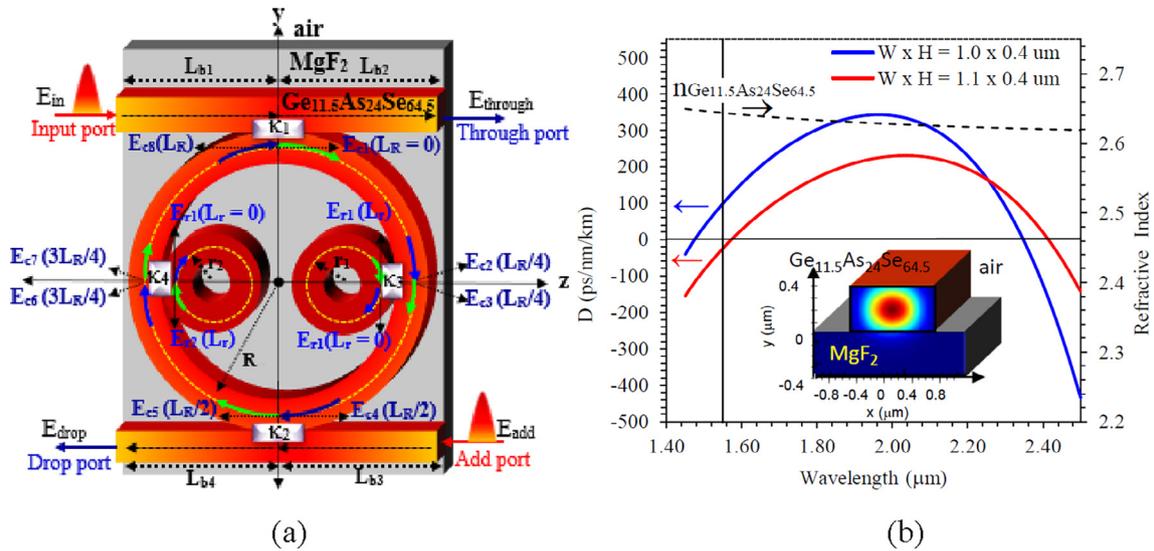
Introduction

Supercontinuum (SC) generation is an important spectrum width that simultaneously covers a wide spectral range of applications in molecular fingerprint spectroscopy, optical coherent tomography, broadband sources and spectroscopy [1–3]. One of the applications has received a lot of interests that has increasingly become a focus for research is the broadband mid-infrared (MIR) SC generation. This is because the amplitudes of bond vibration increase when absorbing MIR light of the same frequency due to oscillation frequencies of bright MIR light sources that match the frequencies of characteristic vibrations of molecular bonds. A nonlinear material as chalcogenide glass (ChG) has recently emerged as a special material with unique properties to provide MIR transparency with selenides transmitting 0.7–33 μm [4]. This material has a large ultra-fast nonlinearity amongst other glass materials, which make them attractive for the real device fabrications and applications in SC generations [5]. High optical and thermal stability can be obtained, where the intense illuminations are applied by using

the Ge$_{11.5}$As$_{24}$Se$_{64.5}$ glass which has the excellent film-forming properties [6]. Also, it was used in the design and optimizing planar waveguides for SC generations with suitably designing GVD tailored to fall in the zero-dispersion wavelength (ZDW) region close to the central wavelength of the pump [7,8].

The nonlinear materials play an important role in photonic crystal fibers, optical waveguide and optical ring resonators [9–12], which has experienced a revolutionary development on the variety of applications such as optical filters, optical sensing, modulators, laser, broadband sources, telecommunications, SC generation and so on [13–15]. In these studies, a Kerr nonlinearity is assumed in such a way, the refractive index varies in response to the optical intensity instantaneously [16–18]. Due to compactness and suitability of the ring resonator waveguides, these devices have recently attracted considerable attention for the integrated photonics circuit applications. Recently several experimental and theoretical investigations were reported such as, in the case of the optical waveguide for SC generation in silicon nanowire, As$_2$S$_3$ chalcogenide planar waveguide, ChG planar waveguides [19–21]

Fig. 1. (a) Schematic diagram of the $Ge_{11.5}As_{24}Se_{64.5}$ Chalcogenide Panda-ring resonator and the definition of electric fields (b) Simulation result, where (Color online) dispersion and $n_{Ge11.5As24Se64.5}$ (dashed curve). The vertical dotted line denotes wavelength of 1.55 μm, (inset) the ridge waveguide geometry. For the fundamental TE mode, It denotes the mode field of the waveguide with W = 1.1 μm, H = 0.4 μm.

etc. SC generations were generated by launching a femtosecond pulse polarized (soliton) in the nonlinear waveguide. The input pulse excites the fundamental mode, which can propagate in the forms of either self-phase modulation in normal dispersion regime or higher-order soliton fission in anomalous dispersion regime. This means, that the resulting spectral output range depends on high input peak power, but the output peak is low in the time domain. In addition, intensity-dependent non-linear ring resonators have been experimentally demonstrated by making use to enhance their effects with cumulative nonlinearities [22–28].

In our study, we have demonstrated the PANDA ChG ring resonator made of optical ChG waveguide consists bus waveguides and ring resonators as shown in Fig. 1(a). It can be used to create a good-quality SC generation of both spectral bandwidth and high output peak power which it can be generated by cumulative nonlinearities. The ChG waveguide geometries were designed from a dispersion-engineered $Ge_{11.5}As_{24}Se_{24.5}$ glass rectangular channel waveguide with air on top and MgF_2 glass. MgF_2 glass is used as a lower cladding material. In order to obtain the ZDW close to the pump wavelength with FDE, the dispersions were tailored. Consequently, the numerical simulation of both the bus waveguides was performed. The GNLS with SSFM has been used for the computations [29,30]. The ring resonators analyses analysis has been performed under the Kerr nonlinearity conditions utilizing the iterative method [31–34]. The ChG Panda-ring resonator is created on both principles that the dynamic transmission properties can be calculated. Thus, the ChG Panda-ring resonator is an important key to combine ultrafast optics and to apply compact on-chip ultra-wide optical broadband SC technologies.

Numerical analysis of nonlinear Panda ring resonators

Fig. 1(a) shows the schematic diagram of the ChG Panda-ring resonator made of the $Ge_{11.5}As_{24}Se_{64.5}$ Chalcogenide glass rectangular channel waveguides designed with air on top, where the MgF_2 glass is used as the lower cladding material. The bus waveguide has a length of L_b (= nλ), where the ring waveguide has a length of L_R (= 2πR = nλ), and the right and left rings have length of $L_{r,1}$ (= 2πr = nλ/4), where R and r are the ring radius, n is an integer, λ is the pumped wavelength and κ is the coupling coefficient. To generate the SC, the dispersion of the waveguide play an important role due to its specific geometry that can be tailored to fall in the near ZDW with a suitable design on a material dispersion. The wavelength-dependent linear refractive indices

of $Ge_{11.5}As_{24}Se_{64.5}$ and MgF_2 [35] glasses were obtained using the Sellmeier equation over the ranges of wavelength applied in the simulation. The finite difference Eigenmode solver was used to calculate the mode dispersion of the ChG waveguide over the wavelength range. The effective mode index is $n_{eff} = \lambda\beta(\omega)/2\pi$ where $\beta(\omega)$ is the propagation constant and the effective mode area is $A_{eff} = |\int (E \times H^*) \cdot \hat{z} dA|^2/|\int (E \times H^*) \cdot \hat{z}|^2 dA$ at the pump wavelength. Subsequently, the used parameter for numerical calculation of GVD is D $(\lambda) = -(\lambda/c) (d^2n_{eff}/d\lambda^2)$ (ps nm^{-1} km^{-1}) curve. This is fitting the dispersion data regarding the Taylor series expansion of up to 10th dispersion as shown in Fig. 1(b).

The coupling mechanism is used to access the looped optical waveguide which is part of the Panda-ring resonator. The constructive interference occurs if the wave round-trip the loop and the phase shift will reach an integer times 2π, so that the cavity is in resonance. The refractive index can be given by

$$n= n_0 + n_2 \ I= n_0 + \frac{n_0 n_2 |E|^2}{2\eta_0} = n_0 + \frac{n_2 P}{A_{eff}} \qquad (1)$$

where n_0 and n_2 are the linear and nonlinear refractive indexes, respectively. I is the optical intensity and P is the optical power. A_{eff} is the effective mode core area of the device.

The linear and nonlinear refractive indices are defined as n_0 and n_2 respectively [36,37], the optical electric field is E and the optical power propagating within the waveguide is P, where the wave impedance in a vacuum is defined as η_0. The propagation in the bus waveguides of length L_b of the Panda-ring resonator is generated by launching a soliton pulse. Its evolution is governed by the GNLSE with SSFM solve. The cavity fields at the end, for the case, if the pulse has slowly varying envelope [1,5,21], can be expressed by

$$\frac{\partial E_b(z,T)}{\partial z} = -\frac{\alpha}{2}E_b(z,T) + \sum_{m \geq 2}^{\infty} \frac{i^{m+1}\beta_m}{m!} \frac{\partial^m E_b(z,t)}{\partial T^m} + i\delta\left(1 + \frac{i}{\omega_0}\frac{\partial}{\partial T}\right)$$
$$\times \left(E_b(z,T) \int_{-\infty}^{\infty} R(T)|E_b(z,T-T')|^2 dT'\right) \qquad (2)$$

where $E_b(z,T)$ and α are the electric field amplitude and the linear propagation loss, respectively. The retarded time frame which is defined as $T = t - z/v_g$ is moving with the group velocity $v_g = 1/\beta_1(\omega_0)$ at the pumped frequency ω_0. The $\beta_m(\omega_0)$ (m ≥ 2) is mth order dispersion parameter. The nonlinear parameter is $\delta = 2\pi n_2/\lambda_0 A_{eff} + i\beta_{TPA}/2A_{eff}$. Here the two-photon absorption coefficient is

β_{TPA}. The material response functions are the instantaneous electronic response $R(t) = [(1 - f_R)\delta(t) + f_R h_R(t)]$ and the delayed Raman responses $h_R(t) = [(\tau_1^2 + \tau_2^2)/(\tau_1\tau_2^2)\exp(-t/\tau_2)\sin(-t/\tau_1)]$ where the parameter of ChG glass are the fractional contribution $f_R = 0.148$, the delayed Raman response $\tau_1 = 23$ fs and $\tau_2 = 164.5$ fs [21,38]. At the coupling point between the ring and the bus waveguides, the complex electric field can be shown in Fig. 1(a). The field amplitudes of incident wave $E_{in}(t)$ transmitted wave $E_{trough}(t)$ and the field amplitudes of incident wave $E_{add}(t)$ transmitted wave $E_{drop}(t)$, and circulating cavity wave $E_{c1}(L_1 = 0,t)$ and $E_{c5}(L_5 = L_R/2,t)$, respectively, satisfy the following equations.

$$E_{through}(z = 0, t) = \sqrt{1-\gamma}\left[\sqrt{1-\kappa_1}E_{in}(z = L_{b1}, t) - i\sqrt{\kappa_1}E_{c8}(L_R, t)\right] \quad (3)$$

$$E_{c1}(z = 0, t) = \sqrt{1-\gamma}\left[-i\sqrt{\kappa_1}E_{in}(z = L_{b1}, t) + \sqrt{1-\kappa_1}E_{c8}(L_R, t)\right] \quad (4)$$

$$E_{drop}(z = 0, t) = \sqrt{1-\gamma}\left[\sqrt{1-\kappa_2}E_{add}(z = L_{b3}, t) - i\sqrt{\kappa_2}E_{c4}(L_R/2, t)\right] \quad (5)$$

$$E_{c5}(z = 0, t) = \sqrt{1-\gamma}\left[-i\sqrt{\kappa_2}E_{in}(z = L_{b3}, t) + \sqrt{1-\kappa_1}E_{c4}(L_R/2, t)\right] \quad (6)$$

where κ is the intensity coupling coefficient of the coupler and γ is the fractional intensity loss. In the following formulation, we have ignored the group-velocity dispersion effect because the length of the ring is short. Moreover, recently, several experimental and theoretical investigations were reported a micro-ring optical to generate robust optical frequency comb, a key process behind frequency comb formation is related to the Kerr micro-ring father than GVD. This is supported by the appearance of signal and idler terms for four-wave mixing (FWM) [39,40]. The ChG glasses have response time 10–20 ms with respect to their slow nonlinearity. This is attributed to photostructural changes inherent rather than free-carrier effects or thermal effects [41–43]. There are a low nonlinearity and waveguide dispersion for the ChG materials due to owning a large effective area. Including low two-photon absorption and absence nonlinear losses of the ChG glass due to free-carriers [44].

The cavity field inside the quarter ring $E_{c2}(L_2 = L_R/4,$ t$)$, $E_{c4}(L_4 = L_R/2,$ t$)$, E_{c6} $(L_6 = 3L_R/4,$ t$)$ and $E_{c8}(L_8 = L_R,$ t$)$ at the end of each ring range can be expressed by the prior cavity field $E_{c(n-1)}(L_{n-1},$ t $- \tau_R)$ at the entrance by considering the instantaneous Kerr effect and the linear loss of the ring, where n = 2, 4, 6, 8, correspondingly, satisfy the following equations

$$E_{c(n)}(L_{n,t}) = E_{c(n-1)}(L_{n-1}, t-\tau_R)\exp(-(\alpha/2)$$
$$(L_n)\exp[-i(\phi_0 + \phi_{N(n-1)}(t-\tau_R)] \quad (7)$$

The propagation distance is defined as L, the quarter round-trip time in the cavity is $\tau_R = n_0 c(L_R/4)$, the amplitude attenuation coefficient of the ring is α, the nonlinear phase shift is $\phi_N(t - \tau_R)$, where the linear phase shift is ϕ_0 $(= n_0 k_0 L_R/4, k_0 = 2\pi/\lambda_0)$. Therefore,

$$\phi_{N(n-1)}(t-\tau_R) = \frac{n_0 n_2 k_0}{2\eta_0}\int_{L_{n-1}}^{L_n}|E_{c(n-1)}(L, t-\tau_R + n_0 L/c|^2 dL$$
$$= \frac{2\pi n_2}{\lambda_0 A_{eff}}\frac{\exp(-\alpha L_{n-1}) - \exp(-\alpha L_n)}{\alpha}|E_{c(n-1)}(L_{n-1}, t-\tau_R|^2 \quad (8)$$

The cavity field inside the right-left quarter ring cavity $E_{c3}(L_3 = L_R/4,$ t$)$ and $E_{c7}(L_7 = 3L_R/4,$ t$)$, respectively. $E_{c2}(L_R/4,$ t$)$ is the incident wave field amplitudes, where the transmitted wave is $E_{c3}(L_R/4,$ t$)$; $E_{c6}(3L_R/4,$ t$)$ is the field amplitudes wave, where $E_{c7}(3L_R/4,$ t$)$ is the transmitted wave; $E_{r1}(L_{r1} = 0,$ t$)$ and $E_{r3}(L_{r3} = 0,$ t$)$ are the circulating cavity waves, which satisfy the following conditions

$$E_{c3}(L_R/4, t) = \sqrt{1-\gamma}\left[\sqrt{1-\kappa_3}E_{c2}(L_R/4, t) - i\sqrt{\kappa_3}E_{r2}(L_r, t)\right] \quad (9)$$

$$E_{r1}(L_r = 0, t) = \sqrt{1-\gamma}\left[-i\sqrt{\kappa_3}E_{c2}(L_R/4, t) + \sqrt{1-\kappa_3}E_{r2}(L_r, t)\right] \quad (10)$$

$$E_{c7}(3L_R/4, t) = \sqrt{1-\gamma}\left[\sqrt{1-\kappa_4}E_{c6}(3L_R/4, t) - i\sqrt{\kappa_4}E_{r4}(L_r, t)\right] \quad (11)$$

$$E_{r3}(L_r = 0, t) = \sqrt{1-\gamma}\left[-i\sqrt{\kappa_4}E_{c6}(3L_R/4, t) + \sqrt{1-\kappa_4}E_{r4}(L_r, t)\right] \quad (12)$$

The fields inside the right and left ring in the cavity of the round-trip time are the E_{r2} $(L_{r2} = L_r,$ t$)$ and $E_{r4}(L_{r4} = L_r,$ t$)$, respectively, the nonlinear phase shifts are $\phi_{Nr(m-1)}(t - \tau_R)$ where m = 2, 4, respectively, which are given by

$$E_{rm}(L_r, t) = E_{r(m-1)}(L_{r(m-1)}, t-\tau_R)\exp(-(\alpha/2)(L_r))\exp[-i(\phi_0$$
$$+ \phi_{Nr(m-1)}(t-\tau_R)] \quad (13)$$

$$\phi_{Nr(m-1)}(t-\tau_R) = \frac{2\pi n_2}{\lambda_0 A_{eff}}\frac{1 - \exp(-\alpha L_r)}{\alpha}$$
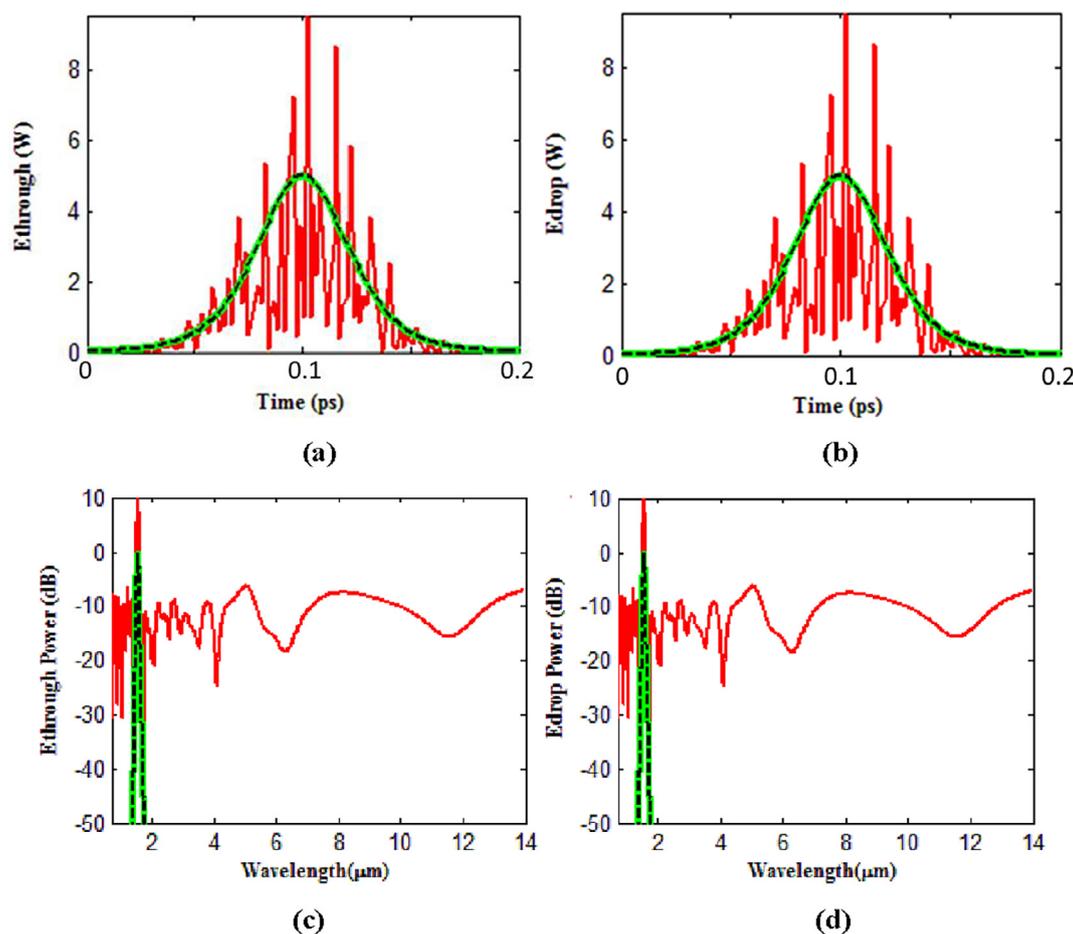$$|E_{r(m-1)}(L_{r(m-1)}, t-\tau_R|^2 \quad (14)$$

From Eqs. (3) and (5), the c $E_{through}$ (t) and E_{drop} (t) are simply an iteration of the cavity fields $E_{c1}(t)$ and $E_{c5}(t)$, respectively, regarding the cavity round-trip time. Therefore, if the optical pulse of arbitrary temporal profile input into the nonlinear Panda-ring resonator, the dynamic properties of the system can be calculated.

Simulation results and discussion

The numerical simulations for the dynamic properties of SC generation in our optimized ChG Panda-ring resonator were carried out by solving the Eqs. (2) to (14) with both SSFM and iteration method for the bus waveguides and the ring resonator, respectively. The SC generation requires a dispersion of channel waveguides exhibiting a near zero-dispersion. The waveguide core can be determined easily by knowing the dimensions of the waveguide such as the W (width) and the H (height). We have investigated the GVDs for three different structures for the fundamental TE mode by using the Sellmeier equation, where the numerical results are presented. For the pump near 1550 nm, using the Lumerical software the curve fitted the dispersion data with respect to the Taylor series expansion which was calculated for up to 10th dispersion. This is shown in Fig. 1(b). The parameter $D = -(2\pi c/\lambda_0)\beta_2$, where for the specific pump power, the W and H have been selected to satisfy the condition as normal GVD, $\beta_2 > 0$. The ChG waveguide has the lowest threshold damage near ZDW regime, where the mode dispersion is normal, therefore SC spectra can simply be broadened by the self-phase modulation. This is shown in Fig. 4 (green online). Thus, we have focused on the ChG waveguide with W = 1100 nm and H = 400 nm. The inset in Fig. 1(b) is presenting the TE mode. We consider the ChG waveguide containing a core of dimensions W = 1100 nm and H = 400 nm with air and MgF$_2$ glass as upper and lower claddings, correspondingly, the numerical result was obtain using the FDE, where the ZDW point is found to be 1.573 μm, while the normal dispersion D = −24.80 ps nm^{-1} km^{-1}, $A_{eff} = 0.39$ μm^2, $\beta_2 = 0.03156$ ps^2 m^{-1}, $\beta_3 = 1.7472 \times 10^{-3}$ ps^3 m^{-1} at the pump wavelength is 1.55 μm, where the second and third-order dispersion are shown by β_2 and β_3 respectively.

The parameters are a sech-shape input pulse of 50 fs duration (FWHM) with peak power between 1 W and 100 W, the nonlinear refractive index $n_2 = 8.6 \times 10^{-18}$ m^2/W [45]. At the pump wavelength of 1.55 μm, the parameters as a linear refractive index and the loss are presented and equal to $n_0 = 2.63$ and $\alpha = 3.2$ dB/cm respectively [46]. The fractional intensity loss $\gamma = 0.1$ and the intensity coupling coefficient $\kappa_1 = \kappa_2 = 0.5$ and $\kappa_3 = \kappa_4$ between 0.1 and 0.9. The Panda-ring resonator consists of the bus waveguide of length $L_b = 2R = 49.338$ μm, the ring radius $R = n\lambda_0/2\pi = 100 \times 1.55 \times 10^{-6}/2\pi \approx 24.669$ μm, the right-left ring radius r = R/4, where n is the integer, which is shown in Fig. 1(a).

Fig. 2 shows the temporal power and SC spectral profiles of the output $E_{through}$ and E_{drop} port with a sech input pulse. The pulse has duration of 50 fs and a peak power of 5 W, where $\kappa_1 = \kappa_2 = \kappa_3 = \kappa_4 = 0.5$, which is incident in nonlinear ChG Panda-ring resonator at 500 round-trips. The SC generation is many short pulses generated through the cumulative nonlinearity by Kerr nonlinearity in the cavity of ChG Panda-ring resonator as shown in both Fig. 2(c) and

Fig. 2. Simulated SC of ChG Panda-ring resonator (a) and (b) Temporal profiles, (c) and (d) SC spectral profiles at the output $E_{through}$ and E_{drop} port (red online), respectively at 500 round-trips for air-clad ChG core employing MgF_2 for its lower cladding the ChG waveguide as pumped wavelength of 1550 nm using 50 fs pulses with 5 W peak power (dashed online) and the output of the bus waveguide length of L_b (green online). The dashed and green online show, for comparison, the corresponding input profiles.
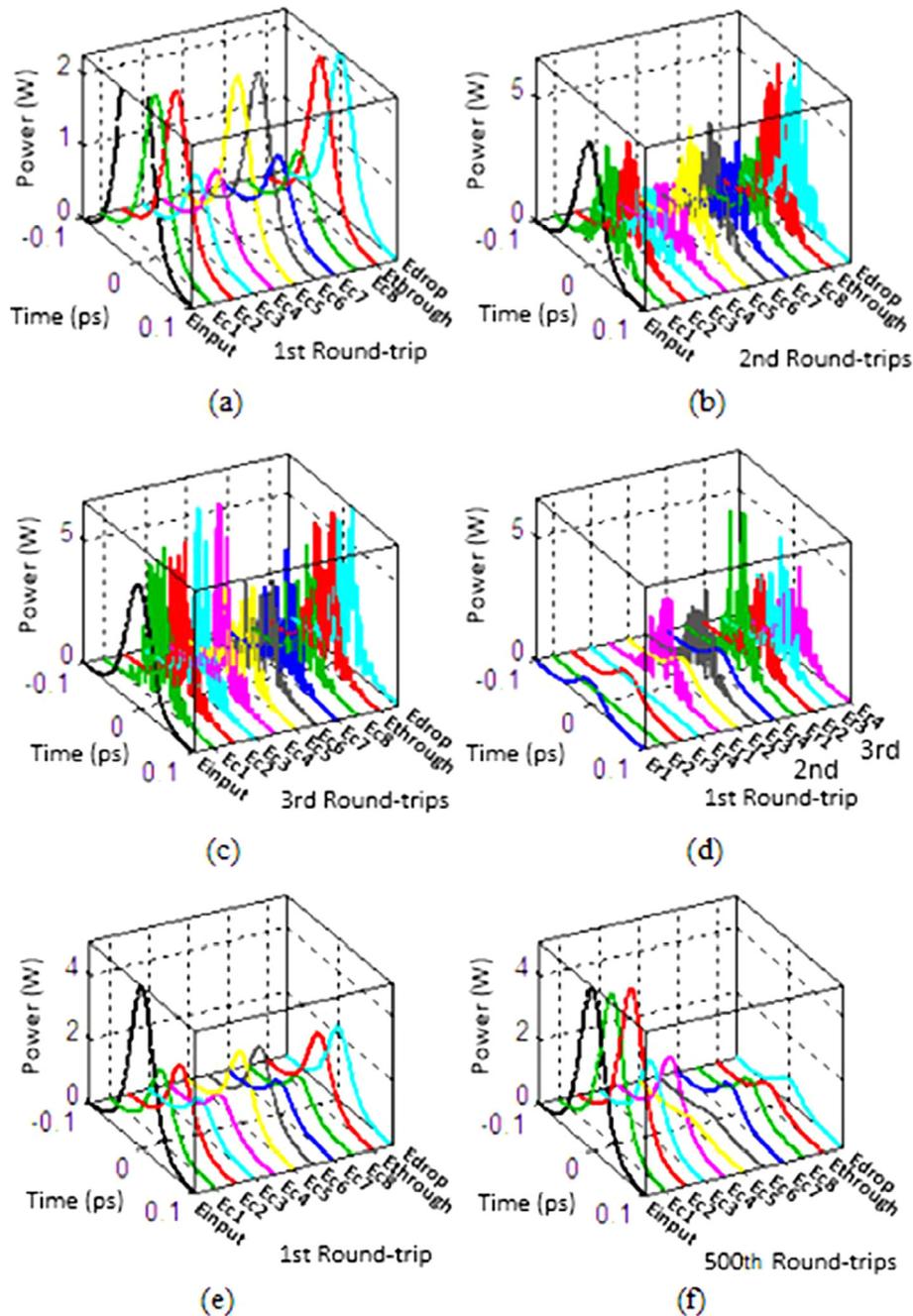
(d), which is both the same. The SC spectrum extends over more than 13 µm (from 0.7 µm to 14 µm) at a −35 dB with the coverage wavelength range from 0.7 µm to 14 µm in Fig. 2(c) and (d). The similarities of both outputs of $E_{through}$ and E_{drop} port can be used as a reference port, which will make for the more diverse applications. For the output bus waveguide length of L_b shows the green online in Fig. 2 due to the dispersion is normal and the bus waveguide is shot. Thus, on solitonic behavior, the temporal and spectral profiles are simply broadened by self-phase modulation.

The numerical result can clearly confirm that the effect to the cumulative nonlinearity for the temporal evolution inside the cavity ring of E_{C1} to E_{C8} and the output $E_{through}$ and E_{drop} port and right and left ring of E_{r1} to E_{r4} for the 1st round-trip, the 2nd round-trip and the 3rd round-trip corresponding to Fig. 2 are shown in Fig. 3(a)–(d). The feature seen here can be understood that the cumulative nonlinearity into the cavity Panda-ring resonator had generated both cases of the many short pulses and the cumulative power in the cavity by the nonlinear phase shift and the resonator of the cavity, a key process for efficient full SC formation. In case the absence of the cumulative nonlinearity ($n_2 = 0$), the temporal profiles are unchanged in simple propagation, which is shown in Fig. 3(e) to (f). Clearly, the primary nonlinear process driving SC generation is cumulative nonlinearity for Kerr response, which differentiates from most of previously reported SC generations that generated by soliton fission, self-phase modulation, four-wave mixing and Cherenkov radiation in both of anomalous and normal dispersion regime.

Fig. 4(a) shows the SC spectra for the ChG Panda-ring resonator,

which is presenting the results for the pump power at 1.55 µm for four different power levels. In the case of 1 W the SC spectrum extends around from 0.7 µm to 14 µm, producing a −35 dB bandwidth over more than 13 µm. After increasing input power level between 5 W and 100 W, the SC spectrum broadened the same input power. Spectral density varies to follow the input power between 1 W and 100 W, where the magnitude of the variations is limited to around 50 dB (from 10 dB to −40 dB), 48 dB (from 10 dB to −38 dB), 55 dB (from 10 dB to −44 dB) and 58 dB (from 10 dB to −48 dB) in Fig. 4(a), respectively. Fig. 4(b) the SC spectra at various coupling coefficients ($\kappa_3 = \kappa_4$) of right-left ring of radius r with a pump wavelength of 1.55 µm at peak power 5 W, all SC spectra extend from 0.7 µm to 14 µm, producing a −40 dB bandwidth over more than 13 µm. Spectral density varies to follow the coupling coefficients of $\kappa_3 = \kappa_4$ ($\kappa_1 = \kappa_2 = 0.5$) between 0.1 and 0.9, where the magnitude of the variations is limited to around 48 dB (from 10 dB to −38 dB), 61 dB (from 10 dB to −50 dB), 53 dB (from 11 dB to −43 dB) and 55 dB (from 10 dB to −45 dB) in Fig. 4(b), respectively. The result is also shown in Fig. 4. Clearly, the various parameters of both the input power and coupling coefficients ($\kappa_3 = \kappa_4$) not affect much of its bandwidth but affect much of its flatness due to the cumulative nonlinearity. The best results are obtained for the SC spectrum with the input power of 5 W and coupling coefficients of 0.5 dotted curves shown in Fig. 4. The noise properties of the flatness SC generation for ChG Panda-ring resonator generated during the process, which can be effectively improved in terms of both of the coherence and intensity stability through the use of a sliding frequency filter.

The Panda-ring resonator can be the efficient full SC generation

Fig. 3. (Color online) temporal of the cavity field wave (a), (b), and (c) the inside ring resonator E_{C1} to E_{C8} and the output $E_{through}$ and E_{drop} port (d) the inside right-left ring of E_{r1} to E_{r4} for the 1st round trip, the 2nd round trip and the 3rd round trip, respectively, (e) and (f) the inside ring resonator E_{C1} to E_{C8} and the output $E_{through}$ and E_{drop} port for the 1st round trip, the 500th round trip, respectively, with $n_2 = 0$. The pump wavelength of 1550 nm using 50 fs pulse with the peak power of 5 W is applied.

such as the expansion of the bandwidth and the increase of the output power (Fig. 2) and the nanostructure. The physical process behind SC generation is related to the Kerr response. This SC can be compared to maximun of 18 octaves at similar wavelength, the straight ChG wave-guide (Fig. 5), Its evolution is governed by the GNLSE (Eq. (2)) with SSFM solve, SC is generated at the output of 10-mm-long ChG wave-guide, the spectral were extended over 1165–1860 nm, bandwidth of 695 nm, with a −35 dB and the maximun output 5.6 W (Fig. 5(b)), a key process for SC generation is related to FWM, soliton fission, self-phase modulation, and Cherenkov radiation. In addition, SC is gener-ated with the Panda-ring resonator. It can also increase output power due to the cumulative ring resonator into the three-ring resonator, i.e. middle and left-right ring resonator, which is different from the straight

waveguide. Moreover, SC generation in ChG using the Panda-ring re-sonator is consistent with a recent experiment using the chalcogenide fiber, which was extended to 1.4–13.3 μm.

The simulation parameters were selected close to the practical de-vice parameters, where the references are given. The use of the chal-cogenide glass in the experimental work is already given. The nonlinear effect is induced into the system. However, the saturation of light en-ergy is balanced by the squeezed energy, which is reported by the au-thors in reference [47], from which the heat dissipation can be released. The device scale and parameters are the practical values, where the references are given. However, this is the simulation work. From the simulation, the crosstalk signals induced by the two side rings are small and suppressed by the resonant output signals as shown in Fig. 2(c) and
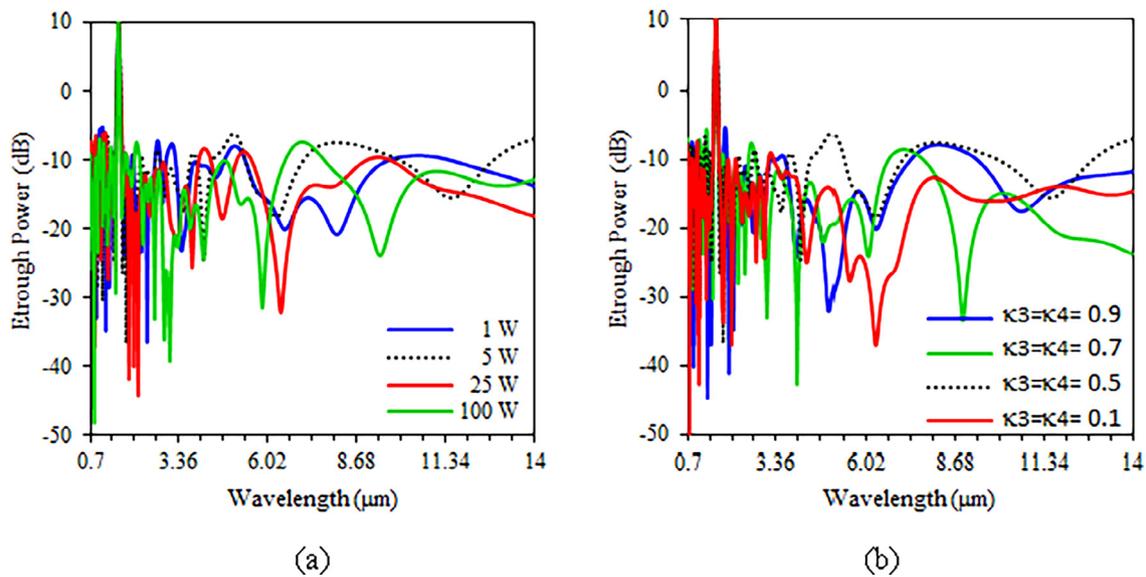
Fig. 4. Simulated SC of ChG Panda-ring resonator of the SC spectral $E_{through}$ port at 500 round-trips at pump wavelength of 1550 nm using 50 fs pulses with $\kappa_1 = \kappa_2 = 0.5$ (a) the peak power between 1 W and 100 W and $\kappa_3 = \kappa_4 = 0.5$, (b) the peak power of 5 W, κ_3 and κ_4 between 0.1 and 0.9.
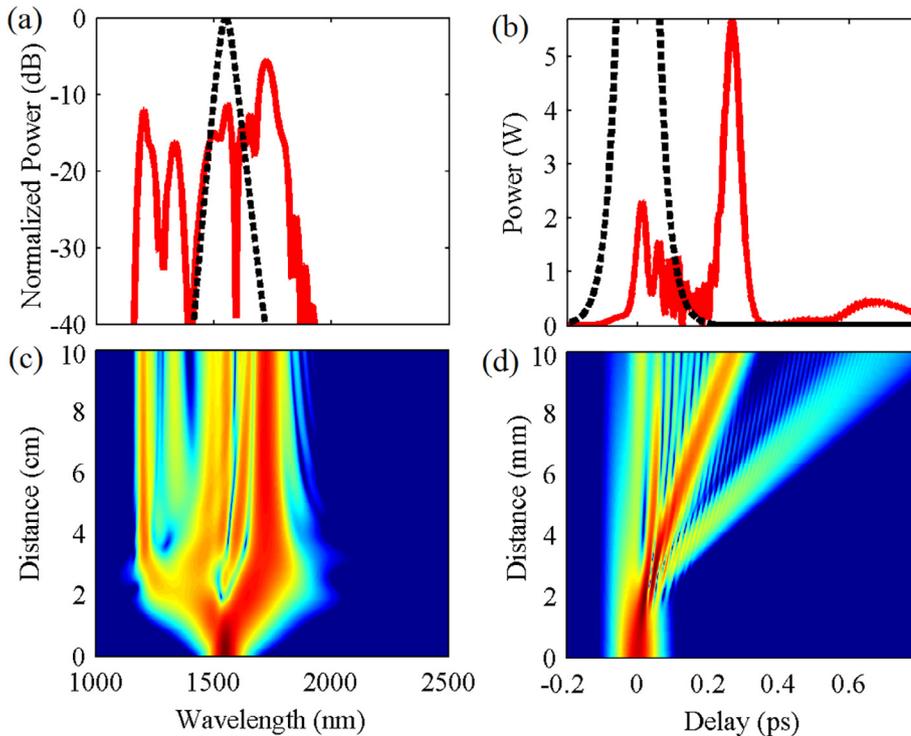

Fig. 5. (Color online) (a) Spectral and (b) temporal profiles at the output of 10-mm-long, and (c) spectral and (d) temporal evolution along the ChG waveguide length, an input 50 fs pulse with 25 W peak power in a $1.0 \times 0.4\,\mu m^2$, air-clad $Ge_{11.5}As_{24}Se_{64.5}$ ChG core employing MgF_2 for its lower cladding, while the anomalous dispersion (solid red line in Fig. 1(b)), $\beta_2 = -1.2572\,ps^2\,m^{-1}$, $\beta_3 = 2.1656 \times 10^{-3}\,ps^3\,m^{-1}$, $A_{eff} = 0.36\,\mu m^2$, at the pump wavelength is $1.55\,\mu m$, while the dotted curves show the input. Other parameter values are the same as those for Fig. 2.

(d). This is the cumulative Kerr nonlinearities, in which the higher order dispersion effect due to the nonlinear existence is already included. The wide range of the output wavelengths can be used for both infrared and radio wave applications.

Conclusion

Generation of SC has been numerically demonstrated by the nanostructure ChG Panda-ring resonator. Using a dispersion engineered to have normal dispersion regime with $D = -24.80\,ps\,nm^{-1}\,km^{-1}$ at a pump wavelength of $1.55\,\mu m$. A sech input pulse of 50 fs duration with peak powers in the range from 1 W to 100 W and coupling coefficients in the range 0.1 to 0.9. The results are obtained for the SC spectrum with low peak power of 5 W (low-energy ≈ 1 pJ) and coupling

coefficients of $\kappa_1 = \kappa_2 = 0.5$ and $\kappa_3 = \kappa_4 = 0.1$, the spectrum is extended over more than $13\,\mu m$ with a -40 dB and has high output peak power. The spectra at various input power and coupling coefficients $\kappa_3 = \kappa_4$, produced a good-quality SC generation from both the spectral bandwidth and high output peak power. The physical process of ChG SC generation is related to the cumulative nonlinearity by Kerr nonlinearity. These studies may have induced new experimental work in the important area of SC generation, which is useful for practical applications and realization of a compact on-chip SC broadband source.

Acknowledgments

Thailand and Ton Duc Thang University, Ho Chi Minh City, Vietnam for the use of laboratory and computer facilities.'

References

[1] Dudley JM, Genty G, Coen S. Supercontinuum generation in photonic crystal fiber. Rev Mod Phys 2006;78:1135.

[2] Hu J, Menyuk CR, Shaw LB, Sanghera JS, Aggarwal ID. Maximizing the bandwidth of supercontinuum generation in As_2Se_3 chalcogenide fibers. Opt Express 2010;18:6722–39.

[3] Aggarwal ID, Sanghera JS. Development and applications of chalcogenide glass optical fibers at NRL. J Optoelectron Adv Mater 2002;4:665–78.

[4] Dantanarayana HG, Abdel-Moneim N, Tang Z, Sojka L, Sujecki S, Furniss D, et al. Refractive index dispersion of chalcogenide glasses for ultra-high numerical-aperture fiber for mid-infrared supercontinuum generation. Opt Mater Express 2014;4:1444–55.

[5] Karim M, Rahman B, Agrawal GP. Mid-infrared supercontinuum generation using dispersion-engineered $Ge_{11.5}As_{24}Se_{64.5}$ chalcogenide channel waveguide. Opt Express 2015;23:6903–14.

[6] Gai X, Han T, Prasad A, Madden S, Choi D-Y, Wang R, et al. Progress in optical waveguides fabricated from chalcogenide glasses. Opt Express 2010;18:26635–46.

[7] Lamont MR, Luther-Davies B, Choi D-Y, Madden S, Eggleton BJ. Supercontinuum generation in dispersion engineered highly nonlinear ($\gamma = 10$/W/m) As_2S_3 chalcogenide planar waveguide. Opt Express 2008;16:14938–44.

[8] Gai X, Madden S, Choi D-Y, Bulla D, Luther-Davies B. Dispersion engineered $Ge_{11.5}As_{24}Se_{64.5}$ nanowires with a nonlinear parameter of $136W^{-1}m^{-1}$ at 1550 nm. Opt Express 2010;18:18866–74.

[9] Ogusu K, Oda Y. Modeling of the dynamic transmission properties of chalcogenide ring resonators in the presence of fast and slow nonlinearities. Opt Express 2011;19:649–59.

[10] Bogaerts W, De Heyn P, Van Vaerenbergh T, De Vos K, Kumar Selvaraja S, Claes T, et al. Silicon microring resonators. Laser Photonics Rev 2012;6:47–73.

[11] Tanaram C, Teeka C, Jomtarak R, Yupapin P, Jalil M, Amiri I, et al. ASK-to-PSK generation based on nonlinear microring resonators coupled to one MZI arm. Procedia Eng 2011;8:432–5.

[12] Amiri I, Alavi S, Ali J. High-capacity soliton transmission for indoor and outdoor communications using integrated ring resonators. Int J Commun Syst 2015;28:147–60.

[13] Singh N, Hudson DD, Yu Y, Grillet C, Jackson SD, Casas-Bedoya A, et al. Midinfrared supercontinuum generation from 2 to 6 μm in a silicon nanowire. Optica 2015;2:797–802.

[14] Amiri I, Soltanian M, Alavi S, Ahmad H. Multi wavelength mode-lock soliton generation using fiber laser loop coupled to an add-drop ring resonator. Opt Quant Electron 2015;47:2455–64.

[15] Alavi S, Amiri I, Ahmad H, Supa'at A, Fisal N. Generation and transmission of 3×3 w-band multi-input multi-output orthogonal frequency division multiplexing-radio-over-fiber signals using micro-ring resonators. Appl Opt 2014;53:8049–54.

[16] Amiri I, Ali J. Generating highly dark–bright solitons by Gaussian beam propagation in a PANDA ring resonator. J Comput Theor Nanosci 2014;11:1092–9.

[17] Amiri I, Alavi S, Soltanian M, Fisal N, Supa'at A, Ahmad H. Increment of access points in integrated system of wavelength division multiplexed passive optical network radio over fiber. Sci Rep 2015;5:11897.

[18] Soltanian M, Amiri I, Alavi S, Ahmad H. All optical ultra-wideband signal generation and transmission using mode-locked laser incorporated with add-drop microring resonators. Laser Phys Lett 2015;12:065105.

[19] Gai X, Choi D-Y, Madden S, Yang Z, Wang R, Luther-Davies B. Supercontinuum generation in the mid-infrared from a dispersion-engineered As_2S_3 glass rib waveguide. Opt Lett 2012;37:3870–2.

[20] Yu Y, Gai X, Wang T, Ma P, Wang R, Yang Z, et al. Mid-infrared supercontinuum generation in chalcogenides. Opt Mater Express 2013;3:1075–86.

[21] Karim M, Ahmad H, Rahman BA. All-normal-dispersion chalcogenide waveguides for ultraflat supercontinuum generation in the mid-infrared region. IEEE J Quantum Electron 2017;53:1–6.

[22] Van V, Ibrahim T, Absil P, Johnson F, Grover R, Ho P-T. Optical signal processing using nonlinear semiconductor microring resonators. IEEE J Sel Top Quantum Electron 2002;8:705–13.

[23] Schwelb O. Transmission, group delay, and dispersion in single-ring optical resonators and add/drop filters-a tutorial overview. J Lightwave Technol 2004;22:1380–94.

[24] Ibrahim TA, Grover R, Kuo L, Kanakaraju S, Calhoun L, Ho P. All-optical AND/NAND logic gates using semiconductor microresonators. IEEE Photonics Technol Lett 2003;15:1422–4.

[25] Tanaram C, Phatharacorn P, Chiangga S, Yupapin P. Analytical and simulation results of micro-ring resonator system using two eyes imaging model. Int J Sci World 2015;3:227–38.

[26] Chiangga S, Suwanarat S, Phatharacorn P, Yupapin P. Super-continuum generation of an optical pulse in a silicon micro-ring resonator. Opt Quant Electron 2016;48:495.

[27] Ogusu K. Dynamic behavior of reflection optical bistability in a nonlinear fiber ring resonator. IEEE J Quantum Electron 1996;32:1537–43.

[28] Li H, Ogusu K. Analysis of optical instability in a double-coupler nonlinear fiber ring resonator. Opt Commun 1998;157:27–32.

[29] Agrawal GP. Nonlinear fiber optics. Nonlinear science at the dawn of the 21st century. Springer; 2000. p. 195–211.

[30] Malomed BA. Variational methods in nonlinear fiber optics and related fields. Prog Opt 2002;43:71–194.

[31] Amiri I, Naraei P, Ali J. Review and theory of optical soliton generation used to improve the security and high capacity of MRR and NRR passive systems. J Comput Theor Nanosci 2014;11:1875–86.

[32] Amiri I, Alavi S, Fisal N, Supa'at A, Ahmad H. All-optical generation of two IEEE802. 11n signals for 2$\backslash$times $2 MIMO-RoF via MRR system. IEEE Photonics J 2014;6:1–11.

[33] Amiri I, Nikoukar A, Ali J. GHz frequency band soliton generation using integrated ring resonator for WiMAX optical communication. Opt Quant Electron 2014;46:1165–77.

[34] Amiri I, Ebrahimi M, Yazdavar AH, Ghorbani S, Alavi S, Idrus SM, et al. Transmission of data with orthogonal frequency division multiplexing technique for communication networks using GHz frequency band soliton carrier. IET Commun 2014;8:1364–73.

[35] Bass M. Handbook of optics. McGraw-Hill; 2000.

[36] Teeka C, Songmuang S, Jomtarak R, Yupapin P, Jalil M, Amiri I, et al. ASK-to-PSK generation based on nonlinear microring resonators coupled to one MZI arm. In: AIP conference proceedings; 2011. p. 221–223.

[37] Alavi S, Amiri I, Idrus S, Supa'at A, Ali J, Yupapin P. All-optical OFDM generation for IEEE802. 11a based on soliton carriers using microring resonators. IEEE Photonics J 2014;6:1–9.

[38] Liu L, Cheng T, Nagasaka K, Tong H, Qin G, Suzuki T, et al. Coherent mid-infrared supercontinuum generation in all-solid chalcogenide microstructured fibers with all-normal dispersion. Opt Lett 2016;41:392–5.

[39] Wang W, Chu ST, Little BE, Pasquazi A, Wang Y, Wang L, et al. Dual-pump Kerr micro-cavity optical frequency comb with varying FSR spacing. Sci Rep 2016;6:28501.

[40] Pu M, Ottaviano L, Semenova E, Yvind K. Efficient frequency comb generation in AlGaAs-on-insulator. Optica 2016;3:823–6.

[41] Shinkawa K, Ogusu K. Pulse-width dependence of optical nonlinearities in As_2Se_3 chalcogenide glass in the picosecond-to-nanosecond region. Opt Express 2008;16:18230–40.

[42] Ogusu K, Shinkawa K. Optical nonlinearities in As_2Se_3 chalcogenide glasses doped with Cu and Ag for pulse durations on the order of nanoseconds. Opt Express 2009;17:8165–72.

[43] Ogusu K, Oda Y. Transient absorption in As_2Se_3 and Ag (Cu)-doped As_2Se_3 glasses photoinduced at 1.06 μm. Jpn J Appl Phys 2009;48:110204.

[44] Toupin P, Brilland L, Trolès J, Adam J-L. Small core Ge-As-Se microstructured optical fiber with single-mode propagation and low optical losses. Opt Mater Express 2012;2:1359–66.

[45] Ma P, Choi D-Y, Yu Y, Gai X, Yang Z, Debbarma S, et al. Low-loss chalcogenide waveguides for chemical sensing in the mid-infrared. Opt Express 2013;21:29927–37.

[46] Yu Y, Gai X, Ma P, Choi DY, Yang Z, Wang R, et al. A broadband, quasi-continuous, mid-infrared supercontinuum generated in a chalcogenide glass waveguide. Laser Photonics Rev 2014;8:792–8.

[47] Ali J, Pornsuwancharoen N, Youplao P, Aziz M, Amiri I, Chaiwong K, et al. Coherent light squeezing states within a modified microring system. Results Phys 2018;9:211–4.